

Title	Polysulfide binding to several nanoscale TiO_{2n-1} Magnéli phases by simple synthesis in carbon for efficient and long life, high mass loaded lithium sulfur battery cathodes
Authors	Zubair, Usman;Amici, Julia;Francia, Carlotta;McNulty, David;Bodoardo, Silvia;O'Dwyer, Colm
Publication date	2018-04-06
Original Citation	Zubair, U., Amici, J., Francia, C., McNulty, D., Bodoardo, S. and O'Dwyer, C. (2018) 'Polysulfide binding to several nanoscale TiO_{2n-1} Magnéli phases by simple synthesis in carbon for efficient and long life, high mass loaded lithium sulfur battery cathodes', Chemsuschem, In Press, doi: 10.1002/cssc.201800484
Type of publication	Article (peer-reviewed)
Link to publisher's version	https://onlinelibrary.wiley.com/doi/abs/10.1002/cssc.201800484 - 10.1002/cssc.201800484
Rights	© 2018 Wiley-VCH Verlag GmbH & Co. KGaA, Weinheim. This is the peer reviewed version of the following article: (2018) Polysulfide Binding to Several Nanoscale TiO_{2n-1} Magnéli Phases by Simple Synthesis in Carbon for Efficient and Long Life, High Mass Loaded Lithium Sulfur Battery Cathodes, ChemSusChem, which has been published in final form at https://doi.org/10.1002/cssc.201800484 . This article may be used for non-commercial purposes in accordance with Wiley Terms and Conditions for Self-Archiving.
Download date	2025-07-03 23:38:26
Item downloaded from	https://hdl.handle.net/10468/5868



UCC

University College Cork, Ireland
Coláiste na hOllscoile Corcaigh

CHEMISTRY & SUSTAINABILITY

CHEM **SUS** CHEM

ENERGY & MATERIALS

Accepted Article

Title: Polysulfide Binding to Several Nanoscale TiO_2 $n-1$ Magnéli Phases by Simple Synthesis in Carbon for Efficient and Long Life, High Mass Loaded Lithium Sulfur Battery Cathodes

Authors: Usman Zubair, Julia Amici, Carlotta Francia, David McNulty, Silvia Bodoardo, and Colm O'Dwyer

This manuscript has been accepted after peer review and appears as an Accepted Article online prior to editing, proofing, and formal publication of the final Version of Record (VoR). This work is currently citable by using the Digital Object Identifier (DOI) given below. The VoR will be published online in Early View as soon as possible and may be different to this Accepted Article as a result of editing. Readers should obtain the VoR from the journal website shown below when it is published to ensure accuracy of information. The authors are responsible for the content of this Accepted Article.

To be cited as: *ChemSusChem* 10.1002/cssc.201800484

Link to VoR: <http://dx.doi.org/10.1002/cssc.201800484>

WILEY-VCH

www.chemsuschem.org

A Journal of



FULL PAPER

Polysulfide Binding to Several Nanoscale Ti_nO_{2n-1} Magnéli Phases by Simple Synthesis in Carbon for Efficient and Long Life, High Mass Loaded Lithium Sulfur Battery Cathodes

Usman Zubair^[a], Julia Amici^[a], Carlotta Francia^[a], David McNulty^[b], Silvia Bodoardo^[a], and Colm O'Dwyer^{[b],[c],[d]*}

Abstract: In Li-S batteries, it is important to ensure efficient reversible conversion of sulfur to lithium polysulfide (LiPS). Shuttling effects caused by LiPS dissolution can lead to reduced performance and cycle life. While carbons rely on physical trapping of polysulfides, polar oxide surfaces can chemically bind LiPS to improve the stability of sulfur cathodes. We show a simple synthetic method allowing high sulfur loading into mesoporous carbon, pre-loaded with spatially localized nanoparticles of several Magnéli phase titanium oxide, Ti_nO_{2n-1} . This material simultaneously suppresses polysulfide shuttling phenomena by chemically binding Li polysulfides onto several Magnéli phase surfaces in a single cathode, and ensures physical confinement of sulfur and LiPS. The synergy between chemical immobilization of significant quantities of LiPS at the surface of several Ti_nO_{2n-1} phases, and physical entrapment ensures Coulombically efficient, long cycle life, high capacity and high rate cathode. These cathodes function efficiently at low electrolyte to sulfur (E/S) ratios to provide high gravimetric and volumetric capacities in comparison with highly porous carbon counterparts. Assembled coin cells have an initial discharge capacity of 1100 mA h g⁻¹ at 0.1 C, and maintain a reversible capacity of 520 mA h g⁻¹ at 0.2 C for more than 500 cycles. Even at 1C, the cell loses only 0.06% per cycle for 1000 cycles with Coulombic efficiency close to 99%.

Introduction

Typical Li ion technologies cannot meet the high-energy demands for systems such as smart grids and electrical transportation, as their energy density is practically limited to 300 W h kg⁻¹[1-2]. Li-S batteries emerged as a prospective solution to the issue due to their remarkably high specific energy value (2600 W h kg⁻¹ or 2800 W h L⁻¹) that is >5 times to the available Li ion technology [2-4]. This estimate is based on the quantity of sulfur and realistic energy densities are much lower, hence the need to minimize further fading and inefficiency in Li-S cell development. Natural abundance of elemental sulfur in the Earth's crust make Li-S technology an attractive low cost alternative to Li-ion batteries. Some of setbacks in Li-S technology include: (i) a low degree of sulfur utilization, (ii) quick capacity fading during cycling, (iii) relatively poor rate capability and (iv) a low Coulombic efficiency [1-2]. These limitations mainly arise because of the low conductivity of S₈ (5 × 10⁻¹⁸ S cm⁻¹), the solubility of polysulfide intermediates, shuttling of dissolved polysulfides, and a general lack of morphological restoration of the sulphur-containing host material during long term cycling [2]. As with Li-ion and Li-O₂ for example, developing stable Li metal anodes is also paramount for high performance and stable Li-S cells, and methods to monitor reactions with Li are important in this regard.[5]

The S₈-containing cathode usually discharges over two voltage plateaus; the first plateau appears at a voltage around 2.3 V vs. Li⁺/Li, corresponding to S₈ being reduced to form Li₂S₈ to Li₂S₆, followed by a transition between 2.3 and 2.1 V, which is linked to the conversion of long chain PS to medium chain PS. A second long plateau approximately extends from 2.1 V vs. Li⁺/Li related to transformation of Li₂S₄ to Li₂S₂ and finally to Li₂S. Lithium polysulfides (LiPS) (Li₂S_n, n = 2–8) are freely soluble in many liquid electrolytes and cause the shuttle phenomenon [4] that limits Coulombic efficiency. Both terminus products of active cathode material, namely S₈ and Li₂S, are practically insoluble and poorly conductive [6-7]. There are two main reported approaches to enhance the performance of sulfur cathodes. The first method involves the physical confinement of sulfur, and the second is associated with the chemical binding of LiPS to avoid solubility-mediated shuttling.

Several methodologies were proposed to make sulfur, Li₂S and LiPS available for electrochemical reactions in a stable, efficient and reversible manner. The first innovation for the Li-S system focused on engineering the design of the cathode host materials, where sulfur is typically embedded into ionically and electrically conductive matrices such as porous graphitic carbons [4], [8]. Carbon matrices are lightweight, conductive and provide the scaffold to fix the reaction products, prevent shuttling while making sulphur accessible to electrochemical reactions for charging and discharging. The most commonly reported carbon matrices are microporous [9-10], mesoporous [3, 11] carbons, carbon nanotubes [12-13], carbon nanofibers [14] and arrangements of

[a] U. Zubair, Dr J. Amici, Dr C. Francia, Prof. S. Bodoardo, Department of Applied Science and Technology (DISAT), Politecnico di Torino, C.so Duca degli Abruzzi 24, 10129 Torino, Italy

[b] Dr D. McNulty, Prof. C. O'Dwyer
School of Chemistry, University College Cork, Cork,
T12 YN60, Ireland. *email: c.odwyer@ucc.ie

[c] Prof. C. O'Dwyer
Micro-Nano Systems Centre, Tyndall National Institute, Lee
Maltings, Cork, T12 R5CP, Ireland

[d] Prof. C. O'Dwyer
Environmental Research Institute, University College Cork, Lee
Road, Cork T23 XE10, Ireland

Supporting information for this article is given via a link at the end of the document.

FULL PAPER

graphene^[15-16]. However, the non-polar nature of carbon surfaces limits the ability of LiPS to adsorb and to remain spatially localized^[17]. Alternatively, conductive polymers such as polyaniline^[18], polypyrrole^[13], polycrylonitrile^[19] were also investigated as sulfur hosts, and in some cases could physically immobilize LiPS to mitigate the shuttling effect. Recent studies have involved the use of sulphophilic frameworks such as metal oxides^[17], MXene^[20], C₃N₄^[21], where the LiPS are chemically bound to the positive electrode. Metal oxides such as TiO₂, SiO₂, Al₂O₃, MnO₂, V₂O₃, Cu₂O, V₂O₅, MoO₃ and others may be effective matrices for sulfur and LiPS adsorption, using the intrinsic polar hydrophilic oxide surface for chemical bonding^[17,22]. Metal oxides can interact with LiPS via chemisorption, acid-base interactions, or form a surface-bound active redox mediators^[17] that mimic spatially localised impregnation approaches into porous carbons. As some metal oxides have 2D van der Waals layered crystal structure, and others crystallize with limited specific surface area, they are less promising compared to porous carbons for physically storing large volumetric quantities of sulfur. Additionally, many oxides have a much lower electronic conductivity, and addressing this issue in tandem with a mechanism that competes with impregnation and docking of sulfur and LiPS in carbons, is important for long life Li-S batteries.

Pure TiO₂ was investigated as a means of chemically binding LiPS^[23-24] during cycling. Nazar et al. studied the effect of TiO₂ in carbon-sulfur cathodes, and they found significant improvement in discharge capacity retention^[24]. Zhang et al. reported TiO₂-loaded carbon fiber paper and TiO₂-anchored hollow carbon nanofiber structures as freestanding cathodes with the ability to physically/chemically trap LiPS^[23, 25]. Xu et al. reported TiO₂ loaded carbon-nanotube paper as an interlayer with efficient physical barrier properties bearing chemical affinity for sulfur and its species^[26]. In a recent study, double oxide structures were exploited in which a SiO₂ matrix was used to host sulfur and a TiO₂ shell created a physical and chemical barrier for LiPS, to mitigate shuttling phenomena^[27]. As metal oxides have low conductivity, they severely limit near-unity Coulombic efficiency and make it difficult for a high level of sulfur utilization. Stoichiometric TiO₂ has a low electrical conductivity (i.e. 10⁻¹⁰ S m⁻¹)^[28], but sub-stoichiometric phases of TiO₂ with Ti_nO_{2n-1} stoichiometry, i.e. Magnéli phases, exhibit remarkable improvement in electrical conductance because of planar defects and crystallographic shear planes^[29-32]. These sub-stoichiometric oxides not only exhibit the conductivity comparable to carbon structures but are also stable in electrochemically oxidizing environments^[33]. These Magnéli phase Ti_nO_{2n-1} materials are now being used for several applications including photovoltaics, photocatalysis, fuel cells, solar cells and energy storage devices^[33-35]. Previously, Cui et al. and Lin et al. showed initial demonstrations of Ti_nO_{2n-1} Magnéli phases as host material for Li-S batteries, but both of studies involved complex and critical synthesis processes^[36-38]. Both investigations involved the use of pure hydrogen to achieve oxygen deficient phases of TiO₂. Nazar et al. reported Ti₄O₇/S composite loaded on carbon fibre paper as positive electrode^[39] and the beginning of a general approach to use the polar surfaces of conductive Magnéli phase oxides and other inorganic materials to enhanced surface-mediated redox chemistry for so-called sulphophilic materials. These approaches have issues affecting their viability. First, they involve the use of a pure hydrogen reduction environment, and

require high reduction temperatures that promote the sintering of nanoparticles^[40]. Second, organotitanium synthesis impedes the control on the shape of Magnéli phase nanoparticles as the shape of raw TiO₂ is more difficult to control^[41]. Pure metal oxide cathodes are prone to pulverization, and cells assembled from these cathodes also require a high concentration of electrolyte to realize good performance, which is not appropriate for high gravimetric capacities^[42]. These limitations can be alleviated by integrating metal oxide nanoparticles into lightweight conductive carbon matrices, and rationally controlling nanoscale Magnéli phases concurrently.

In this work, we demonstrate multiple integrated design strategies to form a cost effective and sustainable sulfur-containing electrode of carbon and Magnéli phase Ti_nO_{2n-1}, that offers exceptional long life and good rate performance with high sulphur loading for Li-S batteries. Electrically conductive Magnéli phase Ti_nO_{2n-1} nanoparticle-loaded carbon matrices (Ti_nO_{2n-1}@C/S) were synthesized by simple heat treatment of the mixture of TiO₂ nanotubes and polyvinyl alcohol (PVA) at 1000 °C in inert environment. Carbon from PVA enables carbothermal reduction of TiO₂ to several Ti_nO_{2n-1} Magnéli phases, which have a chemical binding affinity for LiPS. The approach also suppresses the sintering and grain growth in Ti_nO_{2n-1} nanoparticles ensuring high surface area for LiPS docking that mitigates shuttling effect for a high capacity, Coulombically efficient Li-S battery. Sulfur is introduced into the carbon matrix by a simple thermal infusion process, allowing a high areal sulfur loading (>2.3 mg cm⁻²) with effective LiPS adsorption. The cells were efficiently charged and discharged for 1000 cycles up to 1 C, even for low E/S ratio. This study also demonstrates how physical entrapment of porous carbon in addition to the chemical binding capability of several Magnéli phase oxides contribute synergistically to realize long cycle life Li-S batteries.

Results and Discussion

Sulfur-infused Ti_nO_{2n-1} NP loaded carbon electrode formation

The synthesis of sulfur-infused Ti_nO_{2n-1}@C composite, i.e. Ti_nO_{2n-1}@C/S, is schematically summarised in Fig. 1. This approach is useful for single-pot cathode material synthesis, using the scalable robustness of hydrothermal synthesis and the technical superiority of simultaneous carbonization and carbothermal reduction to the required Magnéli phase from TiO₂ directly. Initially, TiO₂ nanotubes were produced by hydrothermal synthesis. In the procedure, the commercial TiO₂ powder was treated with highly concentrated NaOH solution at 120 °C in a Teflon lined autoclave under autogenerated pressure to prepare sodium titanate (Na₂Ti₆O₁₃) nanosheets. After washing in DI water, Na₂Ti₆O₁₃ nanosheets are immersed into dilute solution of HCl, and consequently curl up into H₂Ti₃O₇ nanotubes as shown in the Figure 2a. These nanotubes were first sonicated, and then interspersed into the dispersion of PVA under mechanical stirring. The dried mass of PVA wrapped TiO₂ nanotubes was heated at 1000 °C in quartz glass tube under nitrogen flux, which allowed simultaneous carbonization of PVA and carbothermal reduction of TiO₂. Carbothermal reduction of TiO₂ created a black mass of Ti_nO_{2n-1}-loaded carbon as illustrated in Figure 1.

FULL PAPER

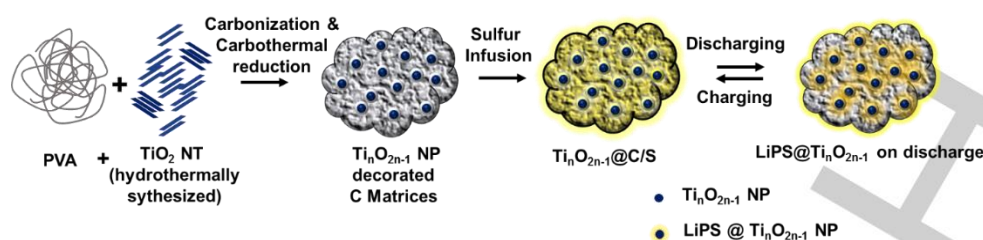


Figure 1. Schematic illustration of the synthesis strategy for carbothermal reduction of TiO₂ nanotubes to Magnéli phase Ti_nO_{2n-1} nanoparticle-embedded carbon host matrices (Ti_nO_{2n-1} NP@C).

The carbon shell on the TiO₂ nanotubes serves two significant purposes during synthesis. First, the carbon porous region provides compartments or incubation sites to spatially localize thermal annealing of TiO₂ nanotubes during their conversion to Magnéli phases. Second, the porous host carbon structures strongly suppress the sintering and grain growth of TiO₂ nanoparticles during carbothermal reduction. Literature reports indicate that a heating temperature below 1050 °C would allow the surface reduction of the rutile TiO₂ phase [34]. Achieving Magnéli phases at 1000 °C using TiO₂ nanotubes was possible because of the high surface area; porous carbon matrices also provide sites for effective thermal reduction, due to the low thermal conductivity and heat loss prevention or carbon. Sintering suppression also ensures TiO₂ nanotubes retain their small dimension when converted to Ti_nO_{2n-1} nanoparticles, and their complete transformation to Magnéli phase Ti_nO_{2n-1}. In the scheme, we indicated the transition from nanotubes to nanoparticle morphology. We incorporate commercially sourced sulfur into Ti_nO_{2n-1}@C using conventional melt diffusion methods at 155 °C to create the Ti_nO_{2n-1}@C/S composite.

Figure 2 details the morphology of as-prepared TiO₂ nanotubes (TiO₂ NT), carbon matrices loaded with Ti_nO_{2n-1} nanoparticles (Ti_nO_{2n-1}@C), and sulfur-infused carbon matrices loaded with Ti_nO_{2n-1} nanoparticles (Ti_nO_{2n-1}@C/S) by FESEM. We observed that TiO₂ NT have a diameter of ~ 10-15 nm with lengths typically ranging from 100 to 300 nm. Secondary electron and backscattered electron FESEM imaging of Ti_nO_{2n-1} NP@C (Figure 2c, 2d) reveals that Ti_nO_{2n-1} nanoparticles are embedded within the carbon matrices.

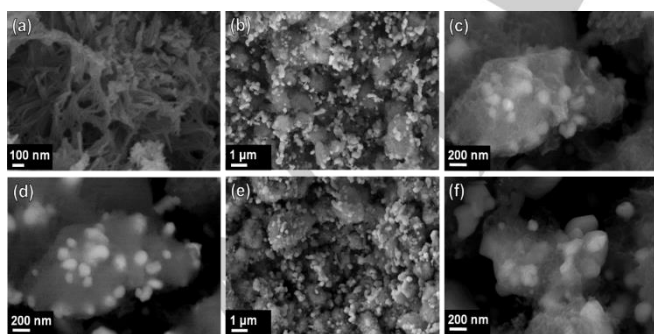


Figure 2. FESEM images of (a) TiO₂ NT (b) Ti_nO_{2n-1}@C, (c) Ti_nO_{2n-1}@C (secondary electron image), (d) Ti_nO_{2n-1}@C (back-scattered electron image), (e) Sulfur-infused Ti_nO_{2n-1}@C/S, and (f) Sulfur-infused Ti_nO_{2n-1} NP@C/S (SE).

During carbothermal reduction, the morphology of the white TiO₂ NT were modified to spherical black Ti_nO_{2n-1} nanoparticles with diameter <100 nm. As pointed out earlier, this morphological transformation occurs from oxygen vacancy formation in the lattice and high-energy thermal reconstruction during hydrothermal treatment to form the Magnéli phase with its corresponding nanoparticle morphology. Meanwhile, the carbonization of PVA provided the carbon matrices with internal Ti_nO_{2n-1} nanoparticles. The carbon matrix efficiently deters the sintering and grain growth of TiO₂, keeping the particle size < 100 nm. From the mass differences of the PVA/TiO₂ composite and the carbothermally reduced composite, it can be inferred that Magnéli phase Ti_nO_{2n-1} is 80% (by mass) of Ti_nO_{2n-1}@C. There is no significant change in morphology after thermal infusion of sulfur into the composite (Figure 2e, 2f), which reflects the homogenous distribution of sulfur into, and onto, the Magnéli-phase converted Ti_nO_{2n-1}@C material.

High-resolution transmission electron microscopy (HRTEM) analysis of typical TiO₂ NTs, Ti_nO_{2n-1}@C matrices and Ti_nO_{2n-1}@C/S composites are shown in Figure 3a-c, respectively. Bright field TEM imaging of TiO₂ NTs confirms a multi-walled tube structure with an external diameter of ~10-15 nm and an internal diameter of 5-8 nm. The NPs of Ti_nO_{2n-1}@C nanoscale constituents have a diameter of ~ 25-30 nm, as shown in Figure 3b and e. Ti_nO_{2n-1}@C/S composites consist of Ti_nO_{2n-1} NPs embedded in composite of C and S (Figure 3c).

A high magnification TEM image of the C/S composite, illustrating its layered structure, is shown in Figure 3f. Selected area electron diffraction (SAED) patterns of TiO₂ NTs, Ti_nO_{2n-1}@C matrices and Ti_nO_{2n-1}@C/S composites were acquired from the areas shown in the inset images in Figure 3h-j, respectively. The SAED pattern for a typical TiO₂ NTs, shown in Figure 3h, indicates a polycrystalline structure of rutile phase TiO₂ (JCPDS No. 21-1276). The SAED pattern for typical Ti_nO_{2n-1}@C matrices consists of a series of polycrystalline rings with d-spacings consistent with Ti₉O₁₇ (JCPDS No. 50-0791). A series of polycrystalline rings with the same d-spacings were observed in the SAED pattern for the Ti_nO_{2n-1}@C/S composite, as shown in Figure 3j, indicating that the titanium oxide present in the NP@C matrices remains as Ti₉O₁₇ during the preparation of the Ti_nO_{2n-1}@C/S composite. The additional diffraction spots present in the SAED pattern for the Ti_nO_{2n-1}@C/S composite, which are not found in the pattern for the Ti_nO_{2n-1}@C matrices, are due to the presence of elemental S. The d-spacings for these diffraction spots are consistent with orthorhombic S₈ (JCPDS No. 08-0247). In this cathode material, the sulfur remained crystalline and stable under electron beam

FULL PAPER

irradiation. EDS elemental mapping confirms that sulfur is homogeneously distributed throughout the composite microstructure (see Supporting Information, Fig. S1). Mapping of Ti indicates that nanoparticles of $\text{Ti}_n\text{O}_{2n-1}$ are well dispersed in the composite just underneath the carbon shell, as sharp boundaries cannot be defined. EDS signals for oxygen directly correspond to the position of $\text{Ti}_n\text{O}_{2n-1}$ nanoparticles. Sulfur signals are comparatively weak over regions where Ti and O signals are quite strong, which highlights that sulfur is initially infiltrated into the carbon matrix and found as separate nanocrystallites, as determined by selected area electron diffraction. Thus, in order to observe the chemical interaction of LiPS with $\text{Ti}_n\text{O}_{2n-1}$ nanoparticles, we obtained EDS analysis of cycled cathodes (vide infra, Fig. 12). Thus, the pre-cycled composite is a carbon matrix loaded with individual $\text{Ti}_n\text{O}_{2n-1}$ nanocrystals with segregated high areal loading of sulfur within the carbon matrix in close proximity.

The microstructure and porosity of the $\text{Ti}_n\text{O}_{2n-1}@C$ matrix and sulfur-infused $\text{Ti}_n\text{O}_{2n-1}@C/S$ composite was quantitatively determined by nitrogen adsorption-desorption curves. Figure 4a demonstrates that the $\text{Ti}_n\text{O}_{2n-1}@C$ matrix has high surface area with a maximum pore size distribution at 5.0 nm. The isotherm in Fig. 4a shows a type IV hysteresis curve indicative of a mesoporous material. The hysteresis shape and the fact we observe no limiting adsorption at high P/P_0 is a particular signature of a composite comprising slit-shaped pores^[43]. This form of porosity in the host material is critical for suppressing shuttling phenomena for improved capacity retention. Moreover, the surface area is significantly reduced from 192 m^2/g to 11.24 m^2/g for sulfur-infused $\text{Ti}_n\text{O}_{2n-1}@C/S$ composite. Importantly, this confirms that sulfur is properly and uniformly infused into pores of the $\text{Ti}_n\text{O}_{2n-1}@C$ matrix. Thermogravimetric analysis (TGA) from room temperature to 800 °C at 10 °C/min under nitrogen atmosphere confirmed that the sulfur loading is ~60% (w/w).

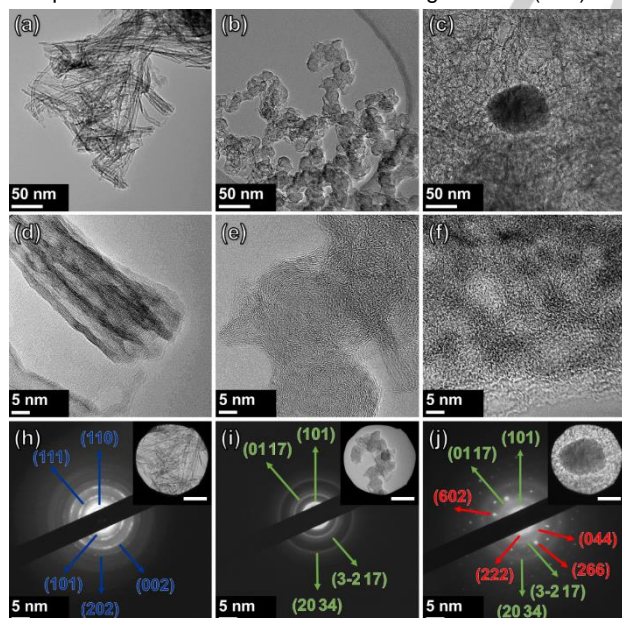


Figure 3. TEM images of (a) TiO_2 NTs, (b) $\text{Ti}_n\text{O}_{2n-1}@C$ matrices and (c) $\text{Ti}_n\text{O}_{2n-1}@C/S$ composites. HRTEM images of (d) TiO_2 NTs, (e) $\text{Ti}_n\text{O}_{2n-1}@C$ matrices and (f) $\text{Ti}_n\text{O}_{2n-1}@C/S$ composites. SAED patterns of (h) TiO_2 NTs, (i) $\text{Ti}_n\text{O}_{2n-1}@C$ matrices and (j) $\text{Ti}_n\text{O}_{2n-1}@C/S$ composites acquired from the areas shown the inset images. The scale bar in the inset corresponds to 50 nm. (Here, Blue corresponds to rutile TiO_2 , green corresponds to Ti_9O_{17} and red corresponds to elemental S).

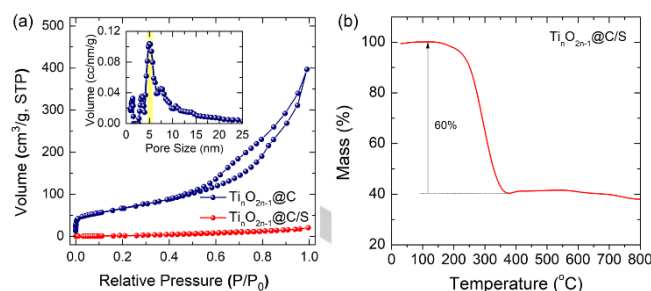


Figure 4. (a) Nitrogen adsorption-desorption isotherms for $\text{Ti}_n\text{O}_{2n-1}@C$ and $\text{Ti}_n\text{O}_{2n-1}@C/S$. (Inset) corresponding pore size measurements. (b) Thermogravimetric analysis of as prepared sulfur-infused $\text{Ti}_n\text{O}_{2n-1}@C/S$ matrix.

Reduction of TiO_2 into Magnéli phase $\text{Ti}_n\text{O}_{2n-1}$ significantly enhanced the electrical conductivity from its rearrangement into the oxygen deficient $\text{Ti}_n\text{O}_{2n-1}$ phases (compared to anatase TiO_2), and from an increase in Ti^{3+} species^[29, 44-45]. Maintaining electrical conductivity to rival graphitic carbon is one benefit of the Magnéli phases, whose surface chemistry also immobilizes LiPS during cycling. XRD data in Figure 5a did confirm that hydrothermal synthesis of TiO_2 NT incorporates rutile phases in pure commercial anatase Hombikat N100 TiO_2 powder, with typical diffraction patterns for nanostructured-layered materials (see Supporting Information, Fig. S2). This polymorph of the material is reported as $\text{TiO}_2\text{-B}$ with edge and corner sharing TiO_6 subunits in the lattice, and exhibits lower density than any of the pure phases of TiO_2 ^[46]. Broadening of the reflections in the diffraction pattern was also confirmed due to dimensional confinement. The carbothermally reduced form of TiO_2 comprised several reflections corresponding to various Magnéli phases of TiO_2 by JCPDS indexing. The XRD pattern agreement showed ~70% coincidence of the reflections with Ti_4O_7 , Ti_5O_9 and Ti_9O_{17} compared with JCPDS files 50-0787, 51-0641 and 50-0791, respectively. The emergence of characteristic peak for Ti_4O_7 at 20.78° was observed in XRD spectrum of $\text{Ti}_n\text{O}_{2n-1}@C$.

The interaction of LiPS with TiO_2 nanotubes and $\text{Ti}_n\text{O}_{2n-1}@C$ matrix was investigated via a visual perception experiment under argon atmosphere. Solutions of different LiPS were prepared by reacting Li_2S and S_8 into a mixture of DME and DIOX over a period of 72 h, under continuous stirring under argon. Figure 5b shows the particularly strong optical adsorption of LiPS onto $\text{Ti}_n\text{O}_{2n-1}@C$ in contrast to solutions of pure TiO_2 NT samples. The LiPS solution containing TiO_2 NT showed a substantial discoloration confirming that TiO_2 also has certain adsorption capability for LiPS as reported in literature [22-25]. This implies that interaction of pure titania may not be adequate for higher sulfur loadings, and low electronic conductivity also limits long cycle life capability. On the contrary, we observe a strong discoloration of concentrated mixture of LiPS in the first 12 h by adding $\text{Ti}_n\text{O}_{2n-1}@C$ into the solution. The strong adsorption of LiPS by $\text{Ti}_n\text{O}_{2n-1}@C$ can be attributed to physical adsorption by porous carbon and in the case of Magnéli $\text{Ti}_n\text{O}_{2n-1}$ oxides, a strong polysulfide interaction is clearly visible, one that fixes LiPS to the oxide surface. Schneider et al.^[47] developed a quantitative UV-vis spectroscopic determined of polysulfide adsorption efficiency on carbon materials, reporting polysulfide contents of 0.04-0.053 g g^{-1} (LiPS in carbon) for carbon and nitrogen-doped carbons in Li-S systems. In our work, for the transparent solution formed after addition of

FULL PAPER

20 mg of $\text{Ti}_n\text{O}_{2n-1}@C$ in 500 μL of a 30 mM Li_2S_6 solution, the approximated adsorption capability of LiPS into the $\text{Ti}_n\text{O}_{2n-1}@C$ matrix is $\sim 0.15 \text{ g g}^{-1}$.

To further probe the electronic and chemical environment, XPS analysis of TiO_2 nanotubes, $\text{Ti}_n\text{O}_{2n-1}@C/S$ composite, charged and discharged cathodes was performed. Figure 5b show the Ti 2p core-level photoemission from TiO_2 NT and $\text{Ti}_n\text{O}_{2n-1}@C/S$ composite. Both materials exhibited two hyperfine split photoemission of titanium oxide compounds at 459 eV and 464.6 eV from $\text{Ti}^{4+} 2p_{3/2-1/2}$. However, $\text{Ti}_n\text{O}_{2n-1}@C/S$ shows two additional and well differentiated lower intensity emissions at 461 eV and 457 eV from $\text{Ti}^{3+} 2p_{3/2}$ and $2p_{1/2}$ that correspond to a specific Ti-S binding [32, 44, 48]. In Magnéli phase $\text{Ti}_n\text{O}_{2n-1}$, surface Ti^{3+} and oxygen vacant sites can interact with oxygen and oxides [49]. Likewise, as Sulfur belongs to same group, it also interacts with Magnéli phase $\text{Ti}_n\text{O}_{2n-1}$ both in elemental and polysulfide form, which is what we detected within the $\text{Ti}_n\text{O}_{2n-1}@C/S$ composite. The S 2p photoelectron emission spectra of as-prepared cathodes and those after 300 charge-discharge cycles (Figure 5d). In our case, the spatially localised composite contain a large starting areal sulfur loading ($>2 \text{ mg cm}^{-2}$), and a high density of Magnéli oxide NPs dispersed throughout the voids and pores in the carbon matrix. The oxides at the electrode scale contain several oxides, all of which are conductive Magnéli oxides that enhance the chemical affinity for LiPS binding during the cycling process. In both cases, the broad core-level emission between 164-172 eV were deconvoluted into two peaks centered at 170.2 eV and 167.7 eV, specifically associated with S-O (SO_2) and S-O (SO_3), respectively. This chemical state is often interpreted as electrolyte degradation, particularly associated with LiTFSI and LiNO_3 electrolyte salts in the absence of TiO_2 [50-52]. According to Umabayashi et al. [53] and Sayago et al. [54] for adsorbed sulfur dioxide (SO_2) molecules on a TiO_2 surface, the typical photoemission from the S 2p states are likewise located between 166 and 170 eV.

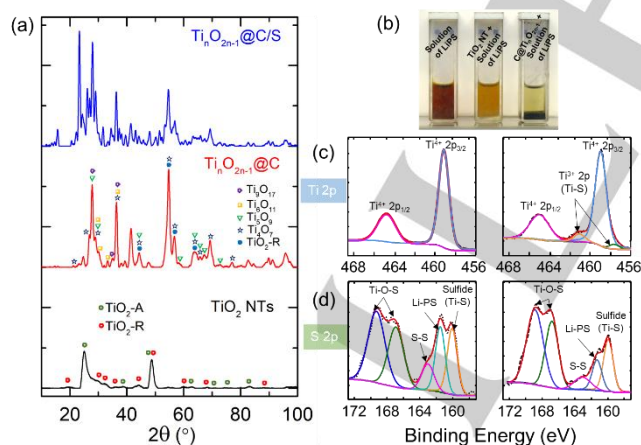


Figure 5. (a) XRD analysis of $\text{Ti}_n\text{O}_{2n-1}@C$ and (c) $\text{Ti}_n\text{O}_{2n-1}@C/S$ composite. (b) Experimental illustration of LIPS adsorption onto Magnéli phases $\text{Ti}_n\text{O}_{2n-1}$ NPs loaded in a carbon matrix, in solution. (c) XPS Ti 2p core-level photoemission spectra of TiO_2 NT, $\text{Ti}_n\text{O}_{2n-1}@C/S$ and (d) S 2p core-level photoemission from charged and discharged $\text{Ti}_n\text{O}_{2n-1}@C/S$ cathodes.

In our case, this XPS signature related to surface-adsorbed $\text{SO}_2 / \text{SO}_3$ molecules from electrolyte decomposition through Ti-O-S bonding at the surface of the Magnéli phase. This interaction is additional to the typical Ti-S bonding in which sulfur atoms have

their S 2p peak between 160.7 and 163.7 eV [31]. This might suggest that carbothermally reduced form of TiO_2 can trap soluble LiPS by a mechanism similar to conversion to polythionate, previously described by Nazar et. al. [17], which increases the adsorption efficiency. However, pure phase Ti_4O_7 is claimed to adsorb PS on its hydrophilic surface only through Ti-S interaction [33]. Our measurements (Fig. 5d) shows that photoemission at ~ 163 and 162 eV originate from S-S and Li-S bonding in LiPS and the peak at 160 eV corresponds to Ti-S binding [31]. Corresponding peaks derived from the Ti-S bond in the Ti 2p and S 2p spectrum after discharge demonstrated the ability of Ti to bond LiPS [55]. We also examined the cathode by XPS after discharging and charging. As the ratio of relative peak intensities of polysulfides (S-S and Li-S) to Ti-O-S decreases in the charged cathode (Fig. 5d) compared to the discharged one (Fig. 8c), we deduce that low order polysulfides are oxidized during the charging process [31]. The Ti-S XPS spectra show that the photoemission intensity associated with strong polysulfide adsorption after charging (i.e. after a complete charge following 300 cycles) is reduced but still present. This suggests that sulfur species maintain interaction with several Magnéli phases of $\text{Ti}_2\text{O}_{2n-1}$ that co-exist within the cathode in NP form for at least 300 cycles [41]. The Ti phases remain as oxides, and TiS_2 or related phases do not form.

3.2. Stable sulfur cathode performance in Li-S cells

To test the electrochemical performance of sulfur-infused $\text{Ti}_n\text{O}_{2n-1}@C/S$ composite, CR2032-type coin cells were assembled. The as-prepared composite was cast on Al foil by mixing with PVDF and Shawinigan Black AB50 (CSW) carbon in ratio of 8:1:1 with sulfur loading of 2-2.3 mg cm^{-2} . The electrolyte to sulfur (E/S) ratio was kept 5-6 $\mu\text{L mg}^{-1}$. Figure 6a shows the stable galvanostatic charging and discharging behaviour of the cathodes at specific current of 334 mA g^{-1} , 836 mA g^{-1} , and 1672 mA g^{-1} (0.2 C, 0.5 C and 1 C, respectively) for 100 cycles. The initial discharge capacities of 1138 mA h g^{-1} , 1100 mA h g^{-1} , 956 mA h g^{-1} , 801 mA h g^{-1} and 700 mA h g^{-1} were reached at specific currents 0.05 C, 0.1 C, 0.2 C, 0.5 C and 1 C respectively. All discharge voltage profiles (Fig. 6b) show two characteristic discharge plateaux. The first, at 2.3 V, is linked to the reduction of sulfur to long chain LiPS, and the second at 2.1 V corresponds to the reduction into short chain LiPS. Figure 6c demonstrates the rate capability of composite cathode at various specific currents. Compared to sulfur-in-carbon electrodes, and the state of the art in conductive oxide host cathodes, we find a high initial capacity with excellent rate dependent response and retention. Even at 1C, following consecutive 10-cycle tests, the cell retains a capacity $\sim 650 \text{ mAh g}^{-1}$ and retains the capacity at each rate, while completely recovering full capacity after switching back to the initial current rate. This indicates the robustness and efficiency of this cathode material even with an order of magnitude higher sulfur loading and low E/S ratio in comparison to previous oxide-based cathodes for Li-S batteries [31-33, 53]. We noted a small polarization effect at higher rates that is also suggestive of encapsulation of Magnéli phase $\text{Ti}_n\text{O}_{2n-1}$ NPs by conductive carbon and structural porosity for quick access of electrolyte.

FULL PAPER

Taking the advantages of higher electronic conductivity of Magnéli phase titania and carbon, and that of nanostructured oxide nanoparticles, the sulfur-infused $\text{Ti}_n\text{O}_{2n-1}@C/S$ composite showed an initial specific capacity of 1050 mA h g^{-1} at 0.2 C with capacity retention of 65% over 500 cycles (Fig. 6d and e). The small reduction in CE is from drying of the cell over the relatively long cycling time. The long cycle performance of the cathode material was also evaluated at the higher rate of 1 C for 1000 cycles as shown in Fig. 6f. At 1 C , cathode material exhibited initial capacity of 700 mA h g^{-1} with less than 0.06% capacity loss per cycle for 1000 cycles with Coulombic efficiency close to 99%. Thus, the cathode synthesis strategy is very efficient in suppressing LiPS dissolution and shuttling by trapping LiPS both physically and chemically, and is capable of long cycle life stable operation with high capacity, and excellent response to faster rates.

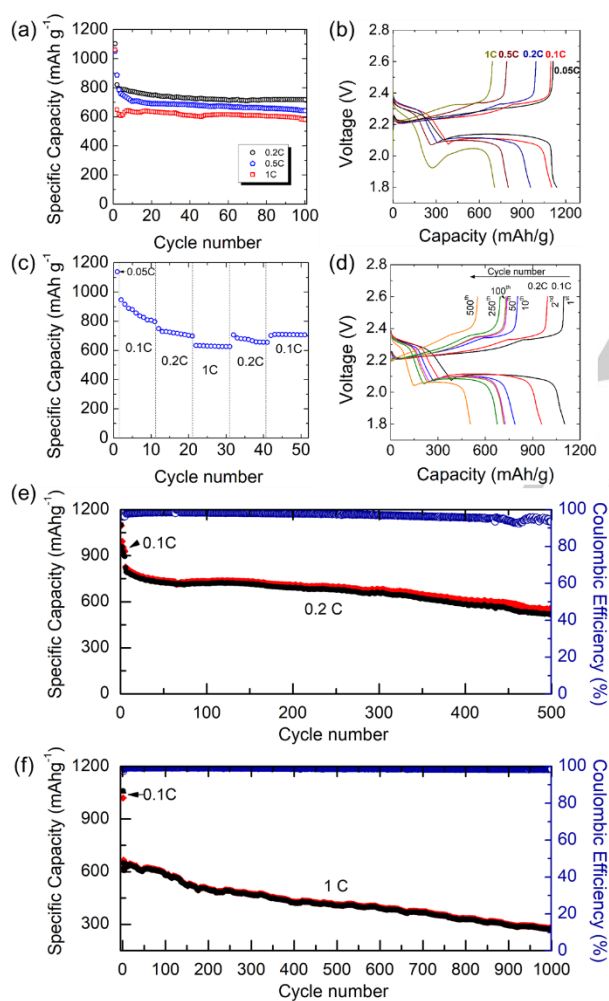


Figure 6. (a) Cycling performance of $\text{Ti}_n\text{O}_{2n-1}@C/S$ NP composite Li-S cathode electrodes at C-rates from 0.2 C to 1 C . (b) Corresponding discharge-charge profiles for each C-rate test. (c) Rate response of the $\text{Ti}_n\text{O}_{2n-1}@C/S$ NP composite at 0.1 C , 0.2 , and 1 C . (d) Corresponding discharge-charge profiles at 0.2 C up to 500 cycles. (e) 500 cycle performance and Coulombic efficiency and (f) Long term cycling behaviour at a high C-rate of 1 C for 1000 cycles.

The cathodes were also cycled voltammetrically (in three electrode configuration using Li^+/Li as reference electrode, Figure

7a) at voltage scan rate of 0.01 mV s^{-1} between 1.5 and 3.0 V to examine the redox characteristics of the cycling process and material electrochemistry. Two distinctive and characteristic cathodic peaks can be observed at 2.35 V and 2.15 V while during oxidation a single large anodic peak appears at 2.45 V . The narrow linewidth of the current (reaction rate) peaks and their consistency confirm good electrical contact and insignificant overcharging behaviour, which we restrict as much as possible by maintaining a discharge voltage window between 1.8 and 2.6 V . Impedance spectroscopic data in Figure 7b of the as-assembled cell at open circuit potential, and after five cycles of charging and discharging, also corroborates the CV and overall cell testing findings. The intercept at high frequency on the real axis implies the equivalent circuit resistance (ESR) of the cell of just 2Ω , confirming the very high electronic conductivity of the cathode-electrolyte interface under electrochemical conditions. Noteworthy is the stable, highly conductive nature of the cycled cathode materials which comprise both metallic (Ti_4O_7) and semiconducting (Ti_6O_{11}) and other $\text{Ti}_n\text{O}_{2n-1}$ phases. On cycling, the R_{ct} value is significantly reduced from 83Ω to 15Ω , signifying reliable solid electrolyte interface (SEI) layer formation [56-57]. Solid-state Li^+ ion diffusion is also enhanced on cycling due to increase in active sites for interfacial electrochemical reaction. This determines the uniform distribution of sulfur, which is further confirmed by EDX mapping of exhausted electrodes (see Fig. 7), and faster Li^+ ion transport into the electrode due to the stable SEI confirmed in XPS analysis.

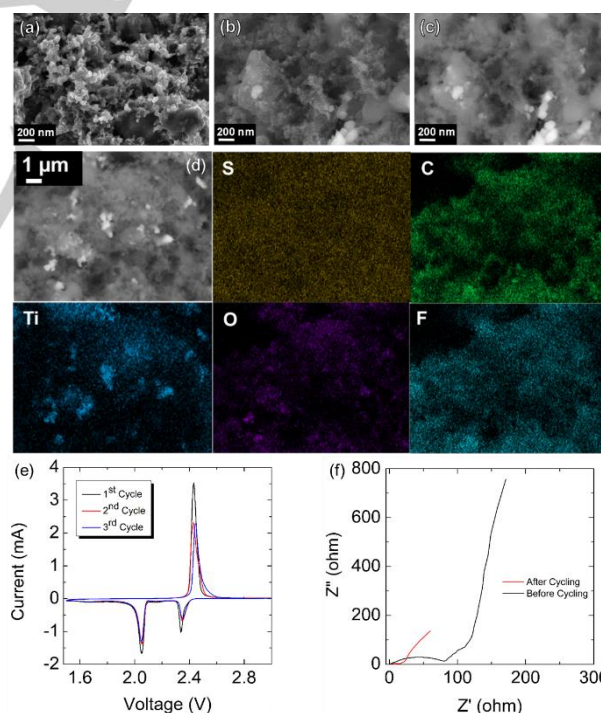


Figure 7. (a-c) FESEM investigation of the surface of Sulfur infused $\text{Ti}_n\text{O}_{2n-1} \text{ NP}@C/S$ cathode after 300 cycles. (d) EDX maps of the exhausted cycled $\text{Ti}_n\text{O}_{2n-1} \text{ NP}@C/S$ cathode material confirming a similar elemental distribution compared to pristine as-synthesized material prior to galvanostatic cycling. (e) First 3 cycles by cyclic voltammetry of sulfur infused $\text{Ti}_n\text{O}_{2n-1} \text{ NP}@C/S$ matrix cathode. A well defined anodic peak at 2.5 V confirms conversion of increasing order polysulfides back to sulfur. (f) Electrochemical impedance spectroscopy of sulfur infused $\text{Ti}_n\text{O}_{2n-1} \text{ NP}@C/S$ matrix cathode.

FULL PAPER

Post mortem analysis of a cycled sample was performed in order to further probe the robustness of the sulfur-infused $\text{Ti}_n\text{O}_{2n-1}@C/S$ cathode. The morphology of fully charged cathode after 300 cycles at 0.2 C was investigated by FESEM and EDX analysis, and confirms a pristine, intact microstructure and porosity of the original composite (Fig. 7), which reflects the ability of our cathode samples to mitigate any large morphological changes. Elemental mapping of the cycled cathode is almost identical to the elemental

Conclusions

In summary, we have demonstrated a facile production strategy to synthesize Magnéli phases of $\text{Ti}_n\text{O}_{2n-1}$ nanoparticles directly within the pores of mesoporous carbon matrices from polymer-encapsulated TiO_2 nanotubes, as an efficient and highly stable sulfur host material. Sulfur loading and Titania NPs are localised and non-aggregated within the carbon host, offering access to electrolyte. The remarkable stability we observe from this cathode is two-fold: the material is morphologically stable with no obvious rearrangement nor deleterious fracturing during long term cycling, and it is also electrochemically stable, where the compositional uniformity and consistency in charge-discharge processes ensures efficient and stable, high capacity Li-S cell operation with high sulfur loading and access to the surfaces of $\text{Ti}_n\text{O}_{2n-1}$ NP. LiPS binding during cycling is possible at the Magnéli phase surface from adjacent sulfur all within the carbon host. The as-synthesized host material can effectively limit the dissolution and shuttling of LiPS by synergetic entrapment of carbon matrix and binding via redox chemistry to several $\text{Ti}_n\text{O}_{2n-1}$ phase nanoparticles simultaneously to achieve extended cycling life. The porous carbon matrix serves to physically entrap sulfur and LiPS, while Magnéli phases titania nanoparticles assist in chemically binding LiPS on their surface. The novel architecture of the host material offers better capacity retention of 55% and 42% at 0.2 C and 1 C for more than 500 and 1000 cycles respectively, with <0.06% capacity loss per cycle at 1 C for 1000 cycles. Moreover, the detailed characterization of synthesized host material and aged cathodes provides an insight that sulfur species are adsorbed by surface of $\text{Ti}_n\text{O}_{2n-1}$ nanoparticles beyond conventional physical entrapment by carbon, and we show that this is general to several Magnéli phases. This strategy offers a facile and scalable manufacturing process to design efficient host materials for high performance Li-S batteries, especially to integrate more surface area of the polar inorganic species, which benefits the cell by LiPS binding compared to just physical entrapment methods typically used. For very electronically conductive oxides such as oxygen deficient Magnéli titania, this work also shows that multiple Magnéli phases can be formed together are more efficient than single phase Ti_4O_7 , without requiring high selectivity during synthesis. The approach may also be possible with other conductive oxide phases that crystallize in Magnéli polymorphs, e.g. V, Mn, Cr, Cu or Mo-based Magnéli oxides among others, and other compounds that have an affinity with sulfur and polysulfides, or that have some redox chemistry with polysulfides.

distribution shown for the as-prepared sulfur-infused $\text{Ti}_n\text{O}_{2n-1}@C/S$ composite in Fig. S1. There is an additional signal from fluorine comes from LiTFSI once SEI layer formation over the cathode is complete. There is sulfur distributed all over the surface, even at regions where the Ti signal is quite intense, conclusively showing a stable material system where sulfur interaction with conductive Magnéli phase $\text{Ti}_2\text{O}_{2n-1}$ occurs.

Experimental Section

Materials Preparation

Preparation of TiO_2 nanotubes: 1 g of commercial anatase TiO_2 powder (Hombikat N100) was dispersed in 10 M NaOH solution (15 ml) under stirring. The mixture was transferred into a Teflon-lined autoclave (25 ml) for hydrothermal reaction. The hydrothermal reaction was carried out at 120 °C for 24 h. The mixture was separated and washed with distilled water five times. The collected mass was dipped in 0.1 M HCl solution for 12 h and subsequently washed with distilled water. The weight of as-prepared nanotubes was 1.076 g.

Carbonization and carbothermal reduction of PVA-wrapped TiO_2 nanotubes: 0.9 g of TiO_2 nanotubes were dispersed in 100 ml of distilled water under sonication. In parallel, 2.3 g of PVA (molecular weight 146-186k) from Sigma Aldrich was dissolved in 400 ml water under continuous stirring at 90 °C. The solutions were mixed under stirring followed by heating at 90 °C for 12 h. The water was evaporated under heating to achieve a solid mixture of the two components. Carbonization and carbothermal reduction of PVA-wrapped TiO_2 nanotubes was carried out by heating at 1000 °C for 1 h at a heating rate 5 °C/min under argon atmosphere with >50 ml/min gas flow in a tubular furnace using pure Ti metal as the oxygen getterer. The weight of final composite was ~1.116 g, and was black in colour.

Preparation of C/S composites: 0.6 g of $\text{Ti}_n\text{O}_{2n-1}$ nanoparticle-decorated carbon was mixed with 0.9 g of sulfur by a pestle and mortar in the ratio of 60:40. The mixture was transferred to an autoclave under argon atmosphere and tightly sealed. Before heating, the mixture was pressed into a disc under high pressure. The vessel was transferred to an oven for 4 h at 120°C and then for 12 h at 155°C, from which the sulfur-infiltrated sample was collected.

Materials Characterization

The morphology of TiO_2 nanotubes, $\text{Ti}_n\text{O}_{2n-1}@C$ matrix and sulfur-infused $\text{Ti}_n\text{O}_{2n-1}@C/S$ composite was examined using field-emission scanning electron microscopy (FESEM, JEOL-JSM-6700F). Transmission electron microscopy analysis was conducted using a JEOL JEM-2100 TEM operating at 200 kV. Energy dispersive X-ray spectroscopy (EDS) of the composites and exhausted cathodes was also performed using JEOL-JSM-6700F to investigate the sulfur presence in the structure of the $\text{Ti}_n\text{O}_{2n-1}@C$ matrix. Sulfur mapping is acquired under FESEM by imaging the X-ray signals from composite surface. The XRD patterns were recorded on a Panalytical X'Pert PRO diffractometer with a PIXcel detector, using Cu K α radiation, under the conditions of $2\theta = 10\text{-}100^\circ$ and 2θ step size = 0.03, to observe the presence of TiO_2 sub-stoichiometric phases. X-ray photoelectron spectroscopy (XPS) measurements were carried out using a Physical Electronics PHI5800 (USA) multi-technique ESCA system, with a monochromatic Al K α X-ray radiation. For testing, the samples were placed in an ultrahigh vacuum chamber at 2×10^{-10} Torr. The porous structures of $\text{Ti}_n\text{O}_{2n-1}@C$ matrix and sulfur-infused $\text{Ti}_n\text{O}_{2n-1}@C/S$ composite were analysed by recording nitrogen adsorption isotherms at 77 K by exposing at a series of precisely controlled relative pressures

FULL PAPER

ranges with an ASAP 2020 Instrument (Micromeritics). Prior to the adsorption measurements, the $Ti_nO_{2n-1}@C$ matrix and sulfur-infused $Ti_nO_{2n-1}@C/S$ composites were degassed at 150 °C and 50 °C (to avoid the sublimation of the sulfur) respectively under vacuum (10 μ m Hg) for 12 h to remove the adsorbates and residual moisture, and then the samples were cooled to nitrogen cryogenic temperature (77K). The specific surface area (SSA) of the samples was calculated by Brunauer–Emmett–Teller (BET) method using Langmuir model within the relative pressure range of 0 to 0.15. The micropore volume and pore size distribution were estimated using density functional theory (DFT) assuming a slit geometry of the pores. Thermogravimetric analysis was carried out with a Mettler Toledo TGA/SDTA 851 instrument by heating the composite at 10 °C min⁻¹ from room temperature to 800 °C.

Electrochemical measurements

For the preparation of the positive electrode, $Ti_nO_{2n-1}@C/S$, CSW carbon and PVDF in a ratio of 8:1:1 were mixed in N-Methyl-2-pyrrolidone (NMP). The slurry was coated on Al foil using a doctor blade with sulfur loading of 2–2.3 mg cm⁻² and dried under vacuum at 50 °C for 10 h. Further details on quantities are summarised in the Supporting Information Table S1. Coin cells (CR2032 type) were assembled in Ar-filled dry glove box (Mbraun Labstar). The geometric area of the electrodes was 2.0 cm². A lithium disc (16 × 0.2 mm, Chemetall s.r.l.) was used as the anode. A Celgard EH2010 (trilayer PP/PE/PP) 19 mm × 0.65 mm soaked with the electrolyte was used as the separator. The electrolyte consisted of 1,2-dimethoxyethane (DME) and 1,3-dioxolane (DIOX) 1:1 (v/v) with 1 M lithium trifluoromethanesulfonate (LiCF₃SO₃, LiTFSI) and 0.25 M LiNO₃. The electrolyte-to-sulfur (E/S) ratio was maintained at 5–6 μ L mg⁻¹ of sulfur. For the purpose of post mortem analysis an ECC-STD electrochemical cell configuration (EL-Cell, GmbH) was employed. Cells were galvanostatically discharged to 1.8 V and charged to 2.6 V by an Arbin BT-2000 battery tester at room temperature. Cycling tests were performed at various C-rate. The C-Rate is calculated using a theoretical capacity of sulfur (i.e. 1672 mAh g⁻¹). Cyclic voltammetry and electrochemical impedance spectroscopy measurements were carried out with a CH Instruments electrochemical workstation using a three-electrode configuration using Li⁺/Li as reference electrode.

Acknowledgements

Financial support was provided by the European Union H2020 NMP-17-2014 ALISE (Grant Agreement 666157). This publication has also emanated from research supported in part by a research grant from Science Foundation Ireland under Grant Number 14/IA/2581.

Keywords: Li-S Battery • sulfur • nanoparticle • energy storage • Magnéli Phase TiO₂ • Lithium • cathode • nanocrystal • electrochemistry

- P. G. Bruce, S. A. Freunberger, L. J. Hardwick, J. M. Tarascon, *Nat. Mater.* **2012**, 11, 19.
- N. S. Choi, Z. H. Chen, S. A. Freunberger, X. L. Ji, Y. K. Sun, K. Amine, G. Yushin, L. F. Nazar, J. Cho, P. G. Bruce, *Angew. Chem. Int. Ed.* **2012**, 51, 9994.
- X. Ji, S. Evers, R. Black, L. F. Nazar, *Nat. Commun.* **2011**, 2, 325.
- A. Manthiram, Y. Z. Fu, S. H. Chung, C. X. Zu, Y. S. Su, *Chem. Rev.* **2014**, 114, 11751.
- A. Jozwiuk, B. B. Berkes, Wei, H. Sommer, J. Janek, T. Brezesinski, *Energy Environ. Sci.* **2016**, 9, 2603.
- D. Zheng, X. R. Zhang, C. Li, M. E. McKinnon, R. G. Sadok, D. Y. Qu, X. Q. Yu, H. S. Lee, X. Q. Yang, D. Y. Qu, *J. Electrochem. Soc.* **2015**, 162, A203.
- M. U. Patel, R. Dominko, *ChemSusChem* **2014**, 7, 2167.
- X. Ji, K. T. Lee, L. F. Nazar, *Nat. Mater.* **2009**, 8, 500.
- U. Zubair, A. Anceschi, F. Caldera, M. Alidoost, J. Amici, C. Francia, M. Zanetti, F. Trotta, S. Bodoardo, N. Penazzi, *J. Solid State Electrochem.* **2017**, 21, 3411.
- X. X. Gu, Y. Z. Wang, C. Lai, J. X. Qiu, S. Li, Y. L. Hou, W. Martens, N. Mahmood, S. Q. Zhang, *Nano Res* **2015**, 8, 129.
- S. R. Chen, Y. P. Zhai, G. L. Xu, Y. X. Jiang, D. Y. Zhao, J. T. Li, L. Huang, S. G. Sun, *Electrochim. Acta* **2011**, 56, 9549.
- Y. Zhao, F. Yin, Y. Zhang, C. Zhang, A. Mentbayeva, N. Umirov, H. Xie, Z. Bakenov, *Nanoscale Res. Lett.* **2015**, 10, 450.
- X. Liang, Y. Liu, Z. Y. Wen, L. Z. Huang, X. Y. Wang, H. Zhang, *J. Power Sources* **2011**, 196, 6951.
- G. Zheng, Q. Zhang, J. J. Cha, Y. Yang, W. Li, Z. W. Seh, Y. Cui, *Nano Lett.* **2013**, 13, 1265.
- G. M. Zhou, L. Li, C. Q. Ma, S. G. Wang, Y. Shi, N. Koratkar, W. C. Ren, F. Li, H. M. Cheng, *Nano Energy* **2015**, 11, 356.
- H. Wang, Y. Yang, Y. Liang, J. T. Robinson, Y. Li, A. Jackson, Y. Cui, H. Dai, *Nano Lett.* **2011**, 11, 2644.
- X. Liang, C. Y. Kwok, F. Lodi-Marzano, Q. Pang, M. Cuisinier, H. Huang, C. J. Hart, D. Houtarde, K. Kaup, H. Sommer, T. Brezesinski, J. Janek, L. F. Nazar, *Adv. Energy Mater.* **2016**, 6, 1501636.
- X. Zhao, H. J. Ahn, K. W. Kim, K. K. Cho, J. H. Ahn, *J. Phys. Chem. C* **2015**, 119, 7996.
- Y. Z. Zhang, S. Liu, G. C. Li, G. R. Li, X. P. Gao, *J. Mater. Chem. A* **2014**, 2, 4652.
- X. Liang, A. Garsuch, L. F. Nazar, *Angew Chem Int Edit* **2015**, 54, 3907.
- Z. Meng, Y. Xie, T. W. Cai, Z. X. Sun, K. M. Jiang, W. Q. Han, *Electrochim. Acta* **2016**, 210, 829.
- X. Gu, C. Lai, *J. Mater. Res.* **2018**, 33, 16.
- Z. Zhang, Q. Li, S. Jiang, K. Zhang, Y. Lai, J. Li, *Chemistry* **2015**, 21, 1343.
- S. Evers, T. Yim, L. F. Nazar, *J. Phys. Chem. C* **2012**, 116, 19653.
- Z. Zhang, Q. Li, K. Zhang, W. Chen, Y. Q. Lai, J. Li, *J. Power Sources* **2015**, 290, 159.
- G. Y. Xu, J. R. Yuan, X. Y. Tao, B. Ding, H. Dou, X. H. Yan, Y. Xiao, X. G. Zhang, *Nano. Res.* **2015**, 8, 3066.
- W. J. Xue, Q. B. Yan, G. Y. Xu, L. M. Suo, Y. M. Chen, C. Wang, C. A. Wang, J. Li, *Nano Energy* **2017**, 38, 12.
- D. Regonini, V. Adamaki, C. R. Bowen, S. R. Pennock, J. Taylor, A. C. E. Dent, *Solid State Ion.* **2012**, 229, 38.
- V. A. Chris R. Bowen, Tony Thomas, presented at International Conference on Mining, Material and Metallurgical Engineering, Prague, Czech Republic, August 11–12, **2014**.
- S. Harada, K. Tanaka, H. Inui, *J. Appl. Phys.* **2010**, 108, 083703.
- X. Y. Zhang, Y. H. Lin, X. X. Zhong, L. J. Wang, W. Y. Liu, A. Singh, Q. Zhao, *J. Mater. Sci.-Mater. El.* **2016**, 27, 4861.
- B. Bharti, S. Kumar, H. N. Lee, R. Kumar, *Sci. Rep.* **2016**, 6.
- H. S. Sutomu Ioroi, Shin-ichi Yamazaki, Zyun Siroma, Naoko Fujiwara, Kazuaki Yasuda, *J. Electrochem. Soc.* **2008**, 155, B321.
- M. Toyoda, T. Yano, B. Tryba, S. Mozia, T. Tsumura, M. Inagaki, *App./ Catal. B-Environ.* **2009**, 88, 160.
- M. M. Zhen, S. Q. Guo, G. D. Gao, Z. Zhou, L. Liu, *Chem. Commun.* **2015**, 51, 507.
- Z. Liang, G. Y. Zheng, W. Y. Li, Z. W. Seh, H. B. Yao, K. Yan, D. S. Kong, Y. Cui, *ACS Nano* **2014**, 8, 5249.
- X. Y. Tao, J. G. Wang, Z. G. Ying, Q. X. Cai, G. Y. Zheng, Y. P. Gan, H. Huang, Y. Xia, C. Liang, W. K. Zhang, Y. Cui, *Nano Lett.* **2014**, 14, 5288.
- C. Yuan, S. Zhu, H. Cao, L. Hou, J. Lin, *Nanotechnology* **2016**, 27, 045403.
- Q. Pang, D. Kundu, M. Cuisinier, L. F. Nazar, *Nat. Commun.* **2014**, 5.
- A. F. Arif, R. Balgis, T. Ogi, F. Iskandar, A. Kinoshita, K. Nakamura, K. Okuyama, *Sci. Rep.* **2017**, 7, 3646.
- T. Takeuchi, J. Fukushima, Y. Hayashi, H. Takizawa, *Catalysts* **2017**, 7.

FULL PAPER

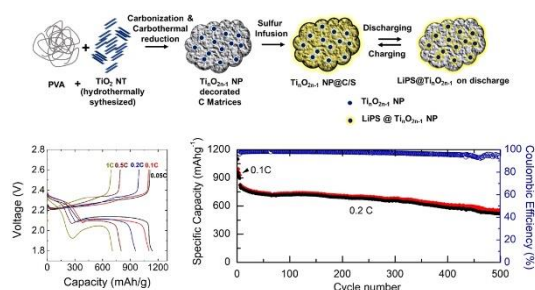
- [42] R. V. Bugga, S. C. Jones, J. Pasalic, C. S. Seu, J. P. Jones, L. Torres, *J. Electrochem. Soc.* **2017**, 164, A265.
- [43] Z. A. AlOthman, *Materials* **2012**, 5, 2874.
- [44] K. Zakrzewska, *Adv. Mater. Sci. Eng.* **2012**, 2012, 13.
- [45] Y. O. Kyung Min Ok, Hiroaki Muta, Ken Kurosaki, Shinsuke Yamanaka, *J. Am. Chem. Soc.* **2017**, 00, 1.
- [46] G. Armstrong, A. R. Armstrong, J. Canales, P. G. Bruce, *Chem. Commun.* **2005**, DOI: 10.1039/B501883H2454.
- [47] A. Schneider, J. Janek, T. Brezesinski, *Phys. Chem. Chem. Phys.* **2017**, 19, 8349.
- [48] T. Q. Lin, C. Y. Yang, Z. Wang, H. Yin, X. J. Lu, F. Q. Huang, J. H. Lin, X. M. Xie, M. H. Jiang, *Energy Environ. Sci.* **2014**, 7, 967.
- [49] T. Hanawa, *J. Periodontal Implan.* **2011**, 41, 263.
- [50] Y. Diao, K. Xie, S. Z. Xiong, X. B. Hong, *J. Power Sources* **2013**, 235, 181.
- [51] D. Aurbach, E. Pollak, R. Elazari, G. Salitra, C. S. Kelley, J. Affinito, *J. Electrochem. Soc.* **2009**, 156, A694.
- [52] Y. Diao, K. Xie, S. Z. Xiong, X. B. Hong, *J. Electrochem. Soc.* **2012**, 159, A1816.
- [53] T. Umabayashi, T. Yamaki, H. Itoh, K. Asai, *Appl. Phys. Lett.* **2002**, 81, 454.
- [54] D. I. Sayago, P. Serrano, O. Bohme, A. Goldoni, G. Paolucci, E. Roman, J. A. Martin-Gago, *Surf. Sci.* **2001**, 482, 9.
- [55] H. Wei, E. F. Rodriguez, A. S. Best, A. F. Hollenkamp, D. H. Chen, R. A. Caruso, *Adv. Energy Mater.* **2017**, 7, 1601616.
- [56] S. S. Yao, S. K. Xue, Y. J. Zhang, X. Q. Shen, X. Y. Qian, T. B. Li, K. S. Xiao, S. B. Qin, J. Xiang, *J. Mater. Sci.-Mater. El.* **2017**, 28, 7264.
- [57] F. R. Qin, K. Zhang, J. Fang, Y. Q. Lai, Q. Li, Z. A. Zhang, J. Li, *New J. Chem.* **2014**, 38, 4549.

FULL PAPER

Entry for the Table of Contents

FULL PAPER

A facile production strategy is able to synthesize Magnéli phases of Ti_nO_{2n-1} nanoparticles directly within mesoporous carbon matrices from polymer-encapsulated TiO_2 nanotubes. These cathode materials act as an efficient and highly stable sulfur host material for Li-S batteries maintaining 520 mAh/g at 1C rate for 1000 cycles.



Usman Zubair, Julia Amici,
Carlotta Francia, David McNulty,
Silvia Bodoardo, and Colm
O'Dwyer*

Page No. – Page No.
**Polysulfide Binding to Several
Nanoscale Ti_nO_{2n-1} Magnéli
Phases by Simple Synthesis in
Carbon for Efficient and Long
Life, High Mass Loaded
Lithium Sulfur Battery
Cathodes**